JOURNAL OF PROPULSION AND POWER
Vol. 24, No. 3, May–June 2008

Rotordynamic Analysis of a Turbopump with the Casing Structural Flexibility

Seong Min Jeon,* Hyun Duck Kwak,† Suk Hwan Yoon,‡ and Jinhan Kim§
Korea Aerospace Research Institute, Daejeon 305-333, Republic of Korea

DOI: 10.2514/1.33551

A critical speed analysis is performed for a 30-ton thrust demonstrator turbopump considering the casing structural flexibility. A full three-dimensional finite-element method including rotor and casing is used to predict rotordynamic behavior. The rotor-alone model and the rotor-casing-coupled model with fixed–fixed and free–free boundary conditions are calculated to investigate the effects of the casing structural flexibility. The stiffness of ball bearings is applied as unloaded and loaded values to consider rotor operating conditions in a vacuum and real engine, respectively. From the results of the numerical analyses, it is found that the effect of the casing structural flexibility reduces the critical speeds of the turbopump. Especially, the loaded rotor condition with higher bearing stiffness is affected dramatically more than the unloaded rotor condition with lower bearing stiffness.

I. Introduction

A LIQUID rocket engine with a turbopump is widely used as a space launch vehicle with a heavy payload to increase the thrust-to-weight ratio compared with a liquid rocket engine with a pressure tank. A turbopump is used to supply high-pressure oxidizer and fuel to a liquid rocket engine. The operating rotational speed of a turbopump is usually very high to reduce the turbopump weight. To drive the turbopump, a turbine is required for generating high power using hot and high-pressure gas. A demonstrator turbopump with a one-axis shaft has been developed for a 30-ton thrust liquid rocket engine [1].

A rotordynamic analysis is mandatory to avoid vibration resonance for a turbopump operation with high speed. The critical speeds of a turbopump are defined as coincidence of the shaft rotating speed and the rotating natural frequencies of the rotordynamic system. Since catastrophic failure is found at the critical speeds due to the resonance, the critical speeds are designed by separating them sufficiently from the turbopump operating speed.

Only a little work has been done in the rotordynamics arena of the liquid rocket engine turbopump. During the development of the space shuttle main engine, research was performed to determine the impact of casing structural effects and bearing nonlinearity on turbopump rotordynamic performance and stability characteristics [2,3]. It was reported that an asymmetric bearing carrier design was shown to improve stability and synchronous response characteristics in the high-pressure fuel turbopump [2] and bearing "dead-band" clearances provided the essential nonlinearity-inducing subsynchronous motion in the high-pressure oxygen turbopump [3]. The transient rotordynamic characteristics of the turbopump used for the Vulcain engine in the Ariane launch vehicle were also studied and compared with the experimental results [4]. The effects of the two kinds of pump seals, the floating ring seal and the plain seal, were investigated on the rotordynamic stability [5].

Until recently, most research has been focused on one-dimensional rotordynamic analysis using the beam finite elements with a lumped mass model, and little work has been done on the three-dimensional rotordynamic analysis using the solid finite elements without any assumption on the model configuration. Especially due to the limitation of the one-dimensional rotordynamic model, a more sophisticated model is required to investigate accurately the effects of casing structural flexibility. In the present study, a rotor coupled with casing is analyzed using a full three-dimensional finite element model. The numerical results are compared with the one-dimensional results to examine the casing effects on the critical speeds by applying fixed–fixed and free–free casing boundary conditions.

II. Rotordynamic Model

A rotor configuration for the analysis is presented in Fig. 1, and several rotating parts are installed the order of nut, front bearing, inducer, impeller, rear bearing, and turbine from the shaft's left end. The lumped mass model of the rotating parts and the stiffness and damping model of the bearings and seals are also depicted in Fig. 1.

As the purpose of the present study is to look into the casing structural flexibility effects on the critical speed, the stiffness and damping model of the seals is disregarded. Unloaded and loaded bearing circumstances are taken into account to estimate the ball bearing stiffness for vacuum environment operation and real engine operation, respectively.

The unloaded bearing stiffness case is for the rotordynamic tests in a vacuum to be performed in the near future. Dynamic force induced by mass unbalance of the rotating parts is considered as the only external force for the unloaded bearing stiffness. The front bearing stiffness is 3.655×10^7 N · m, and the rear bearing stiffness is 4.322×10^7 N · m in vacuum operation.

In real engine operation, the bearings are loaded in the radial and axial direction by the pump hydrodynamic and turbine aerodynamic forces. The bearing stiffness shows nonlinear behavior as a function of the bearing load. The steady-state operating condition is applied for the calculation of the bearing loaded stiffness in the present study. The turbopump driven by the turbine using hot and high-pressure gas rotates at 20,000 rpm at the steady-state operation, and the outlet pressure of the pump approaches up to 140 bar. At this state, the axial and radial loads of the bearings are close to 1 kN and 1.4 kN, respectively. The loads imposed on the bearings bring about the stiffness of 1.498×10^8 N · m for the front bearing and 1.751×10^8 N · m for the rear bearing.

Material, mass, and mass moment of inertia are presented in Table 1 for the rotating parts including the inducer, impeller, and turbine. The z coordinate stands for the rotating axis, and the x and y

Presented as Paper 5543 at the 43rd AIAA/ASME/SAE/ASEE Joint Propulsion Conference and Exhibit, Cincinnati, OH, 8–11 July 2007; received 18 July 2007; revision received 18 January 2008; accepted for publication 23 January 2008.

*Senior Researcher, Turbopump Department, 45 Eoeun-Dong, Yuseong. Member AIAA.
†Researcher, Turbopump Department, 45 Eoeun-Dong, Yuseong.
‡Senior Researcher, Turbopump Department, 45 Eoeun-Dong, Yuseong.
§Head of Department, Turbopump Department, 45 Eoeun-Dong, Yuseong.

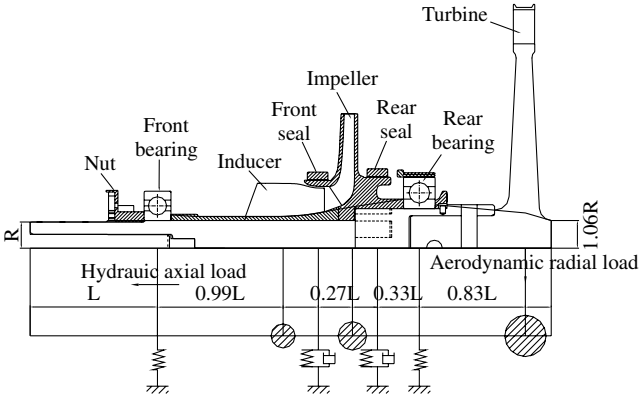

Fig. 1 Rotor configuration of turbopump.

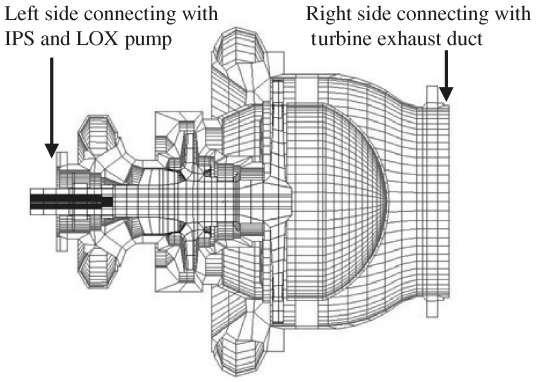

Fig. 2 3-D finite-element model of rotor and casing.

coordinates stand for the transverse axes. I_{zz} is the polar mass moment of inertia, and I_{xx} and I_{yy} are the transverse mass moments of inertia. As for material of the casing parts, stainless steel SS 316 is used for the pump casing, and nickel base alloy Inconel 625 is used for the turbine casing. The mass ratio of the casing to the rotor is 5.613.

A cross-sectional view of the three-dimensional finite-element model is shown in Fig. 2 for the coupled analysis of the rotor and casing.

Each rotor and casing is modeled using 11,000 and 7000 solid elements, respectively. For the convenience of modeling and analysis, nonaxisymmetric features such as the turbine blades and pump casing struts are simplified as axisymmetric models by applying equivalent Young's modulus and density. The bearings are modeled using linear spring elements. Fixed–fixed and free–free boundary conditions are applied on the both left and right end flanges of the casing shown in Fig. 2. These two extreme casing boundary conditions are considered as the upper and lower bounds between which the practical boundary condition is expected to exist.

III. Numerical Analysis

A. Unloaded Condition

Not only the rotor but also the casing natural frequencies are obtained simultaneously from the complex eigenvalue analysis of the rotor-casing coupled model. Dissimilar to the results of the uncoupled analysis, the vibration modes of the rotor and casing are mutually influenced by the structural coupling due to the bearing in the coupled analysis. Only the isolated axial and circumferential modes of the casing are revealed independently of the rotor-bending modes. The rigid-body modes obtained from the eigenvalue analysis are removed in the present results.

Figure 3 shows the first mode shapes of the rotor-alone model and the rotor-casing coupled model without a bearing load at the nonrotating state in the fixed–fixed boundary condition. The rotor-bending mode is dominant in the first rotor-casing coupled mode, and the casing mode is not shown. Nevertheless, the structural effect due to the casing flexibility is reflected in the rotor-casing coupled model contrary to the rotor-alone model with infinite casing stiffness. Equivalent stiffness of the rotor support is softened due to the casing flexibility added on the bearing stiffness, and the relative shaft stiffness to the support stiffness increases. Therefore, the first mode

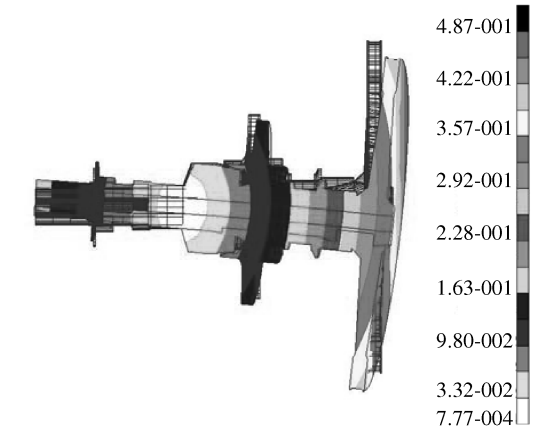

a) Rotor-alone model (220.1 Hz)

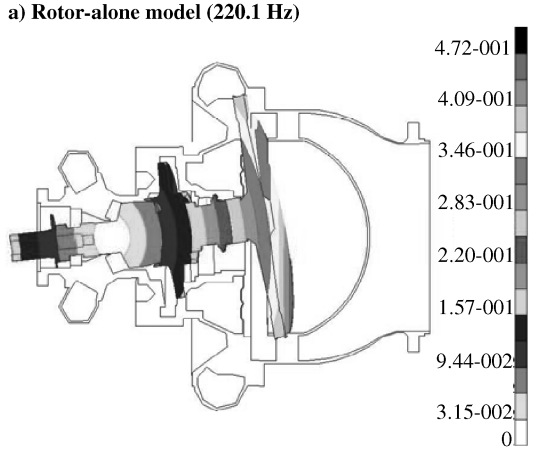

b) Rotor-casing coupled model (205.6 Hz)

Fig. 3 First mode shape without bearing load in the fixed–fixed boundary condition.

Table 1 Mass and mass moment of inertia of rotating parts

	Fuel pump		
	Inducer	Impeller	Turbine
Material	17-4PH	17-4PH	INCONEL 718
Density, g/cm^3	7.64	7.64	8.19
Mass, kg	0.1682	1.446	6.822
$I_{xx} = I_{yy}$, kg · mm^2	96.84	1996	32,770
I_{zz}, kg · mm^2	152.9	3682	65,290

of the rotor-casing coupled model shows more clearly as a rigid-rotor mode compared with the first mode of the rotor-alone model. The first natural frequency is also reduced in the rotor-casing coupled model.

As the rotor starts to rotate, the rotating natural frequencies of the rotor increase due to the gyroscopic effect. The mass unbalance caused by offset of the rotor mass center from the rotating axis of the shaft induces forced vibration with the synchronous rotating frequency. Critical speeds are shown as crossing points between the rotor-rotating natural frequencies and the forcing frequency. Since vibration amplitude of the turbopump with light damping is very large at the critical speeds, more accurate estimation is required for the critical speeds.

Figure 4 shows the rotating natural frequencies of the rotor-alone model and the rotor-casing coupled model with the fixed–fixed and

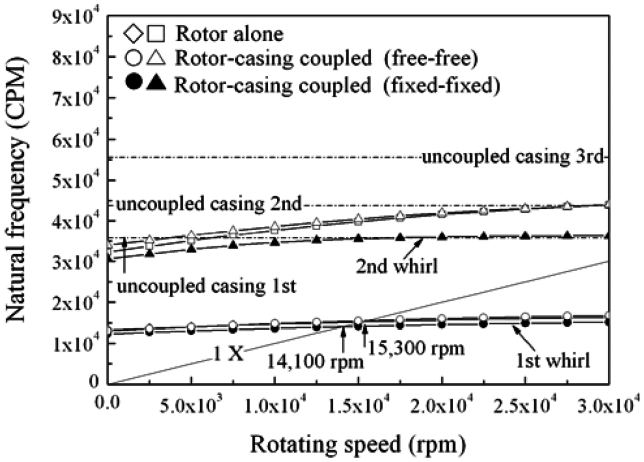

Fig. 4 Campbell diagram without bearing load.

free–free casing boundary conditions. The first and second rotating natural frequencies are compared with the running speeds (1×) and the uncoupled casing natural frequencies.

The first critical speed is 15,300 rpm in the rotor-alone model. The casing flexibility effect decreases the first critical speed down to 14,100 rpm by 7.8% in the rotor-casing coupled model with the fixed–fixed casing boundary condition. On the other hand, the first critical speeds of both the rotor-alone model and the rotor-casing coupled model are almost same in the free–free casing boundary condition. The casing flexibility little affects the critical speeds in that boundary condition.

The first critical speeds without bearing load are summarized in Table 2 for the one-dimensional beam model, three-dimensional rotor-alone model, and three-dimensional rotor-casing coupled model with two casing boundary conditions. The one-dimensional beam model result is additionally presented to examine the casing structural flexibility effect by comparing it with the three-dimensional model results. It is found that the numerical analyses show the same first critical speeds in all of the models except the three-dimensional rotor-casing coupled model with the fixed–fixed casing boundary condition. The fixed–fixed boundary condition reduces the critical speed.

B. Loaded Condition

The turbopump bearings are properly loaded by the axial and radial loads of the rotating parts in normal operation. As previously described, the bearing stiffness under the loaded state is approximately four times larger than the bearing stiffness under the unloaded state.

Figure 5 shows the first mode shapes of the rotor-alone model and the rotor-casing coupled model with bearing load at nonrotating state in the fixed–fixed boundary condition. The rotor natural frequencies increase as the bearing stiffness increases under the loaded state compared with the unloaded state. A shaft elastic bending mode due to the heavy weight of the turbine is more clearly shown in the loaded state. This phenomenon is caused by the lowered relative shaft stiffness to the increased bearing stiffness.

Figure 6 shows the rotating natural frequencies of the rotor-alone model and the rotor-casing coupled model with the fixed–fixed and free–free casing boundary conditions. The rotating natural

Table 2 First critical speeds without bearing load

Numerical model	First critical speed, rpm
1-D beam model	15,300
3-D rotor-alone model	15,300
3-D couple model (free–free)	15,300
3-D couple model (fixed–fixed)	14,100

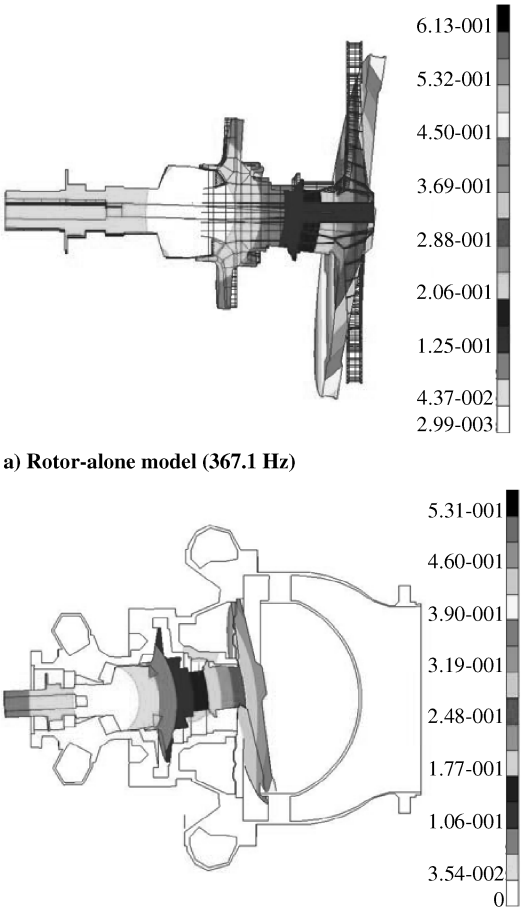

Fig. 5 First mode shape with bearing load in the fixed–fixed boundary condition.

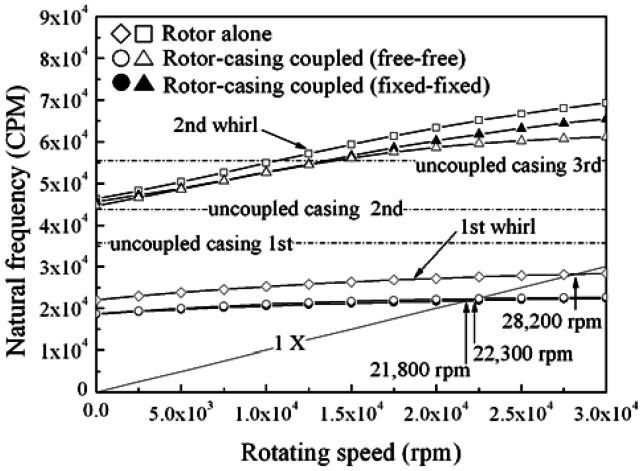

Fig. 6 Campbell diagram with bearing load.

frequencies up to the second are compared with the synchronous running speeds and the uncoupled casing natural frequencies.

Although the absolute critical speeds increase due to the increased bearing stiffness in the loaded state, the effect of the casing flexibility is enlarged more in the loaded state than in the unloaded state by reducing the critical speeds more deeply. The first critical speed is 28,200 rpm in the rotor-alone model with bearing load. The casing flexibility effect decreases the first critical speed down to 21,800 rpm by 23% in the rotor-casing coupled model with the fixed–fixed casing boundary condition. Because of the casing flexibility, the first critical speed reduces by 8% with the unloaded bearing stiffness and

Table 3 First critical speeds with bearing load

Numerical model	First critical speed, rpm
1-D beam model	28,700
3-D rotor-alone model	28,200
3-D couple model (free–free)	22,300
3-D couple model (fixed–fixed)	21,800

by 23% with the loaded bearing stiffness in the fixed–fixed boundary condition. The more the bearing stiffness increases, the more the casing flexibility influences the critical speed with the same boundary condition. As the bearing stiffness relatively increases against the shaft stiffness, the role of the casing rigidity enlarges so that the equivalent support stiffness, which affects the rotordynamic characteristics, decreases.

Contrary to the previous results under the unloaded state with the free–free casing boundary condition, the critical speeds of the rotor-casing coupled model with that boundary condition decrease due to the enlarged effect of the casing flexibility in the increment of the bearing stiffness. As for the free–free casing boundary condition, the first critical speed decreases from the 28,200 rpm of the rotor-alone model to the 22,300 rpm of the rotor-casing coupled model by 21%. It is found that the critical speed drop is revealed both in the fixed–fixed and free–free casing boundary conditions, with the loaded bearing stiffness contrary to the unloaded bearing stiffness.

The first critical speeds with bearing load are summarized in Table 3 for the one-dimensional beam model, three-dimensional rotor-alone model, and three-dimensional rotor-casing coupled model with two casing boundary conditions. With the loaded bearing stiffness, the magnitude of the first critical speed decreases in the order of the one-dimensional beam model, the three-dimensional rotor-alone model, the coupled model with the free–free boundary, and the coupled model with the fixed–fixed boundary.

IV. Conclusions

The critical speed analysis of the turbopump is performed to examine the effect of the casing flexibility using the one-dimensional model, three-dimensional rotor-alone model, and three-dimensional rotor-casing coupled model.

The casing structural flexibility reduces the first critical speed. The numerical results show that the one-dimensional beam model predicts the highest value of the critical speed. The lowest value of the first critical speed results from the three-dimensional rotor-casing coupled model. The three-dimensional rotor-alone model estimates an intermediate value between the results of the two models.

The critical speed of the rotor-casing coupled model is more affected and reduced in the fixed–fixed casing boundary condition compared with the free–free casing boundary condition.

As the bearing stiffness increases, the casing flexibility more deeply influences the critical speed with the same boundary condition. Therefore, the measure of the critical speed reduction is enlarged in the bearing loaded state compared with the bearing unloaded state.

References

[1] Kim, J., Lee, E. S., Choi, C. H., and Jeon, S. M., "Current Status of Turbopump Development in Korea Aerospace Research Institute," *International Astronautical Congress 2004*, SP-17, IAC, Vancouver, Canada, Oct. 2004.

[2] Childs, D. W., "The Space Shuttle Main Engine High-Pressure Fuel Turbopump Rotordynamic Instability Problem," *Journal of Engineering for Power*, Vol. 100, No. 1, 1978, pp. 48–57.

[3] Childs, D. W., and Moyer, D. S., "Vibration Characteristics of the HPOTP (High Pressure Oxygen Turbopump) of the SSME (Space Shuttle Main Engine)," *Journal of Engineering for Gas Turbines and Power*, Vol. 107, No. 1, 1985, pp. 152–159.

[4] Brune, C., and Lassoudiere, F., "Rotordynamics of the Vulcain LH2 Turbopump Comparison Between Test Results and Dynamic Analysis Calculations," *Proceedings of 3rd International Conference on Rotordynamics*, International Federation for the Promotion of Mechanism and Machine Science, Querétaro, Mexico, 1990, pp. 353–360.

[5] Kwak, H. D., Lee, Y. B., Kim C. H., Ha, T. W., and Woo, Y. C., "Prediction of Rotordynamic Stability for a High Pressure High Speed Turbopump Unit," *Proceedings of the 6th International Conference on Rotordynamics*, International Federation for the Promotion of Mechanism and Machine Science, Querétaro, Mexico, 2002, pp. 478–485.

T. Wang
Associate Editor